RSC Advances

PAPER

View Article Online
View Journal | View Issue

Cite this: *RSC Adv.*, 2018, **8**, 34224

Mesoporous silica nanoparticles with wrinkled structure as the matrix of myristic acid for the preparation of a promising new shape-stabilized phase change material *via* simple method

Dian Chen,[a] Yan Chen,[a] Xiuwang Guo,[a] Wenwen Tao,[a] Jinbao Wang,*[a] Shufeng Gao[b] and Junkai Gao *[a]

Wrinkled mesoporous silica nanoparticle (WMSN), with a special and highly uniform morphology, large specific surface area and pore volume, high porosity and radial-like wrinkled channels, was successfully prepared by a simple and easy synthetic method. WMSN was used as the matrix of myristic acid (MA) to prepare a new attractive shape-stabilized PCM (MA/WMSN), and the wrinkled channels of WMSN are useful to prevent the leakage of PCM, and increase the thermal stability and phase change enthalpy of shape-stabilized PCM. Characterizations of MA/WMSN, such as structure, crystallization properties, chemical properties and thermal properties were studied, and the interaction mechanism between the WMSN and MA molecules was elucidated. TGA results suggested that MA/WMSN had excellent thermal stability. When the loading of MA in MA/WMSN was 65%, the melting and crystallizing enthalpies of MA/WSSN were 92.0 J g^{-1} and 86.0 J g^{-1}, respectively. Additionally, the thermal conductivity of MA/WMSN was 0.37 W mK^{-1}, which was about 1.37 times higher than that of the pure MA. All of the study results demonstrated that MA/WMSN possessed of favourable thermal conductivity, high latent heats and excellent thermal stability, and therefore it could be a suitable thermal energy storage material for practical applications.

Received 3rd August 2018
Accepted 28th September 2018

DOI: 10.1039/c8ra06536e

rsc.li/rsc-advances

Introduction

As a result of increasing energy shortage and environmental problems, such as the greenhouse effect, the importance of efficient thermal energy conservation has been highlighted.[1,2] As a type of energy storage material, phase change materials (PCMs) can store or release energy during the phase change process, and it is an important and highly efficient method for saving energy.[3,4] Typically, PCMs can be assigned into inorganic, inorganic–organic composite and organic phase change materials on the basis of their chemical compositions.[3,5] Organic PCMs have been used widely because of their numerous merits, including self-seeding nucleation behavior, favorable thermal and chemical stability, suitable melting temperature range, low cost, and temperate transformation enthalpies.[6–8]

Fatty acids, as one of the numerous organic PCMs, have become a current research hotspot because of their outstanding characteristics, including high heat capacity, suitable range of melting temperature, high surface tension, available and congruent melting, slight volume variation, low degree of supercooling and low commodity cost.[9,10] Among many fatty acids, myristic acid (MA) has a high latent heat and a good melting point. However, leakage during the melting process is a problem facing organic PCMs and limits their energy-saving applications.[6] Preparing shape-stabilized PCMs is an effective way of solving the above issues.[11] There are many types of supporting materials used in preparing shape-stabilized PCMs, including porous materials (*e.g.*, OPP, AC, SBA-15, and MCM-41), polymer networks, metal foams, a variety of graphite materials, and silica materials.[3,11,12]

Specifically, mesoporous silica used as a supporting material for PCMs has attracted the attention of researchers because of its many advantages, such as high surface areas, strong absorption, homogeneous pores and periodical structure.[5,13,14] There were several good reports regarding the use of mesoporous silica as supporting materials for shape-stabilized PCMs. Qian *et al.* conducted a study of radial-like mesoporous silica sphere as supporting material for organic PCMs, and the results indicated that radial-like mesoporous silica is an ideal supporting material for shape-stabilized PCMs.[13] Amaia M. Goitandia *et al.* investigated the thermal cycling behavior of composite materials that used mesoporous silica, bentonite,

[a]*School of Port and Transportation Engineering, Zhejiang Ocean University, Zhoushan 316022, People's Republic of China. E-mail: jinbaow@zjou.edu.cn; gaojk@zjou.edu.cn; Fax: +86 580 2554491; Tel: +86 580 2554491*

[b]*Yinzhou Kefeng New Material of Polymer Co. Ltd., Ningbo 315100, People's Republic of China*

diatomaceous earth, expanded graphite or zeolites as matrix materials. The results showed that mesoporous silica with nanosized pores could reduce the risk of PCM leakage, and shape-stabilized PCMs could be used in building materials without a protective layer for preventing leakage.[15] However, in actual applications, it was usually difficult for the target materials to enter into the inside pores of mesoporous silica that had mesopores with capillary tube shapes.[16]

In recent years, the preparation and application of wrinkled mesoporous silica (WMSN), which had special and highly uniform morphology of radial-like channels, high porosity, large specific surface area and pore volume, have become a current research hotspot.[17–19] Especially, the radial-like channels of WMSN could beneficial for the entry of guest materials into the internal channels of the WMSN, and the wrinkled channels of WMSN are useful to prevent leakage, improve loading and increase phase change enthalpy. Therefore, the application of WMSN in the preparation of shape-stabilized PCMs for immobilizing organic PCMs is expected to achieve good performance. However, there are no reports about preparing shape-stabilized PCMs by immobilizing MA in wrinkled mesoporous silica nanoparticles at present. Ongoing efforts are necessary to study the thermal properties of shape-stabilized PCMs using WMSN as the matrix.

Therefore, in this work, wrinkled mesoporous silica nanoparticle was firstly synthesized and then used to immobilize myristic acid to prepare a new shape-stabilized PCM (MA/WMSN) by a simple and easy synthetic method. Characterizations of MA/WMSN were then conducted, and the interaction mechanism between the MA molecules and WMSN was clarified. The study results showed that WMSN with suitable morphology could be an excellent supporting material and the MA/WMSN could be used as a suitable thermal energy storage material for practical applications.

Materials and method

Materials

MA (myristic acid) was used to prepare the composite PCMs, CTAB (cetlytrimethyl bromide), NBA (*n*-butyl alcohol), TEOS, carbamide and CYH (cyclohexane) were purchased from Sinopharm Chemical Reagent Co., Ltd., China. Acetone was purchased from Nanjing Chemical Reagents Co., Ltd., China. Ethanol was purchased from Ji'an Hao MAI Fine Chemical Industry Co., Ltd., China.

Preparation of WMSN

The typical synthesis process for wrinkled mesoporous silica nanoparticle is as follows:[19] 1.0 g CTAB powder, 1.0 g carbamide, 30.0 g NBA, and 12 mL CYH were put into a 100 mL round-bottom flask, and the mixture was stirred slowly for 5 min until the CTAB completely dissolved, and then TEOS was injected into the mixture by a syringe. After that, the bottleneck was sealed up and placed into a water bath. After stirring for 30 min at 25 °C, the mixture was incubated at 70 °C for 20 h. Finally, the mixture was centrifuged, and the precipitates were placed into acetone, and back-flowed at 80 °C for 48 h followed by washing with distilled water to remove acetone. After air-drying, WMSN was obtained.

Preparation of MA/WMSN

MA/WMSN was prepared by vacuum impregnation to increase the load of MA, and the schematic diagram for the preparation of MA/WMSN is shown in Fig. 1. For immobilization of MA onto WMSN, 50 mg of WMSN was placed into a flask connected to a vacuum pump. MA was dissolved in 15 mL of ethanol, and the mixture was placed into the flask. Then the mixture was stirred and meanwhile, the vacuum pump was opened for 1 h. After that the flask was placed into a water bath, and the mixture was stirred at 54 °C for 4 h. Finally, the mixture was dried by putting it into an oven at 54 °C for 24 h, and the MA/WMSN was obtained.

Characterization

TEM (transmission electron microscope, JEM-2100F, JEOL, Japan) was used to obtain images of WMSN, and the surface morphology of MA and MA/WMSN were studied using SEM (scanning electron microscope, Quanta FEG 250, America). Surface-area of WMSN was measured using the Brunauer–

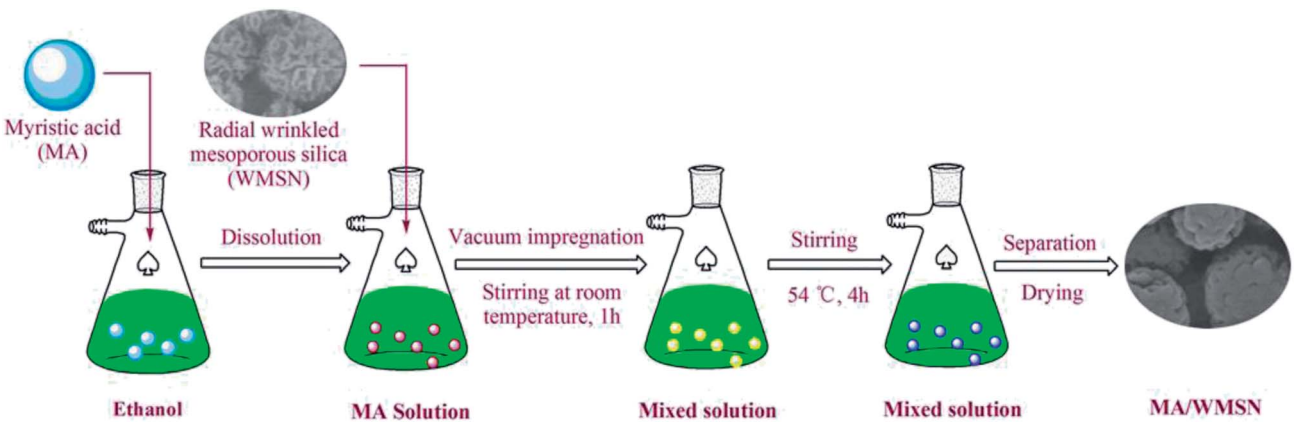

Fig. 1 Schematic diagram for the preparation of MA/WMSN.

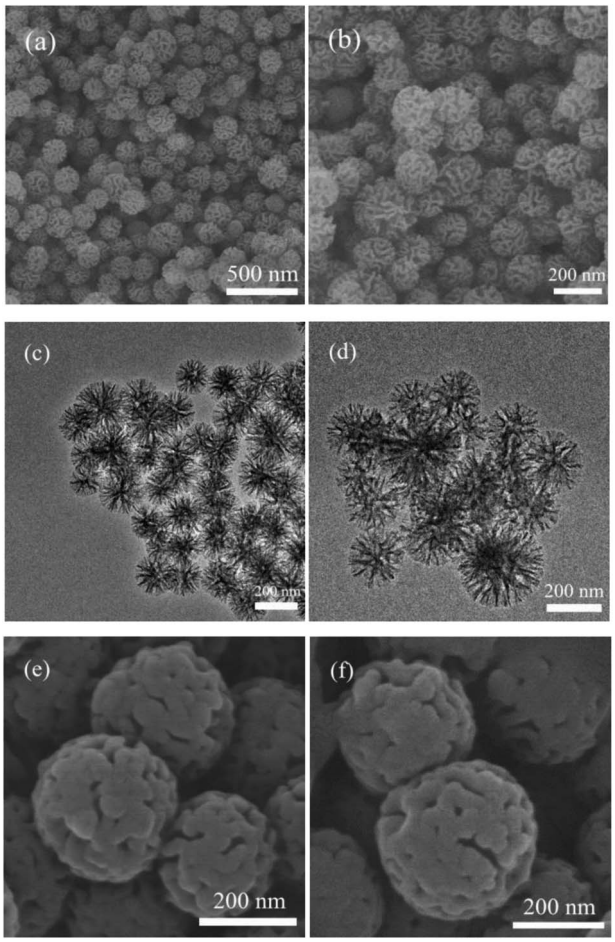

Fig. 2 SEM images of (a) and (b) WMSN, (e) and (f) MA/WMSN and TEM images of (c) and (d) WMSN.

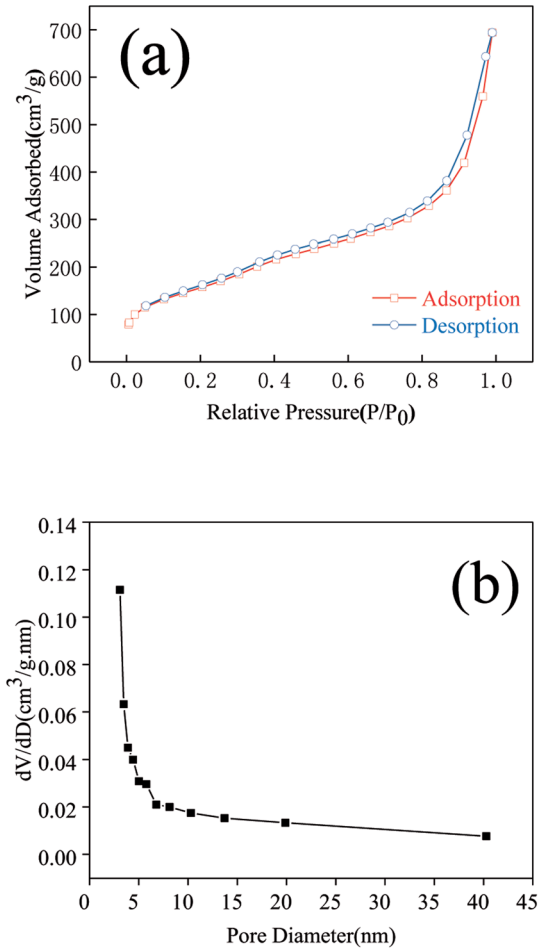

Fig. 3 N_2 adsorption–desorption isotherms (a) and pore size distribution obtained from the adsorption isotherm (b).

Emmett–Teller (BET, Quanta nova 2000e, America) method. XRD (X-ray diffraction, D/MAX-2500, Rigaku, Japan) experiments for MA and MA/WMSN were performed under the same conditions of 40 kV and 30 mA. Thermal stabilities of MA and MA/WMSN were measured by TGA (thermogravimetric analysis) from room temperature to 550 °C at 10 °C min^{-1}. FT-IR spectra of MA, WMSN and MA/WMSN were acquired using a Nicolet6700 spectrometer from Thermo Scientific. Phase change temperature and enthalpies of MA and MA/WMSN were carried out by DSC (Differential Scanning Calorimetry, 200-F3, NETZSCH), and the measurements were performed at a heating and cooling rate of 10 °C min^{-1} and 2 °C min^{-1}, respectively, over a temperature range between 5 °C to 100 °C. The protective and purge gas used during TGA and DSC experiments was high-purity nitrogen. Thermal conductivities of MA and MA/WMSN were measured by a xenon lamp flash thermo thermal conductivity meter (TA DXF-500, America).

Results and discussion

Characterization of WMSN and MA/WMSN

Fig. 2(a), (b), (e) and (f) shows the SEM micrographs of WMSN and MA/WMSN, respectively, and Fig. 1(c) and (d) show the TEM micrographs of WMSN. In Fig. 2(a) and (b), the SEM image of the WMSN shows that the silica nanoparticles had uniform wrinkled morphologies with a narrow size distribution and the diameter of the nanoparticles ranged from 150 nm to 350 nm. The special wrinkled morphology could prevent the leakage of MA and then improve the loading amount of MA/WMSN and increase its phase change enthalpy. In Fig. 2(c) and (d), the TEM image of the WMSN showed that the wrinkled mesoporous silica nanoparticles had radial-like mesopores, which was beneficial for the entry of MA into the internal channels of the WMSN.[16,20] Fig. 2(e) and (f) show SEM images of the MA/WMSN composite. MA was dispersed in the MA/WMSN composite, which was beneficial for the surface tension forces between MA and the porous net of WMSN. In addition, the structure of the WMSN provided a fine mechanical strength for the MA/WMSN. At the same time, the wrinkled channels prevented the leakage of MA during the melting process, and the large pore volume of WMSN could benefit the accommodation of organic phase change materials.

Fig. 3(a) shows a type IV isotherm nature with a hysteresis loop characteristic of WMSN in the P/P_0 range of 0.05 to 0.99, which was indicated that WMSN had mesoporous

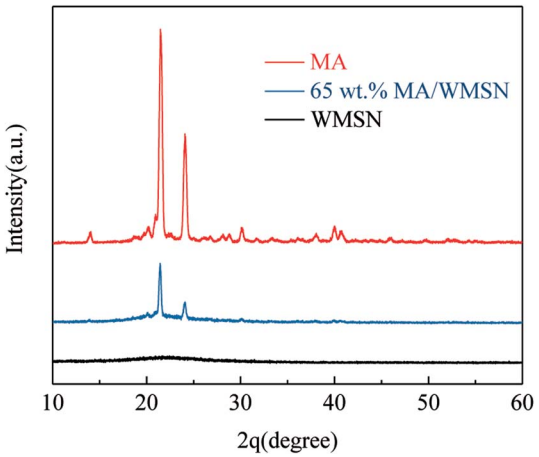

Fig. 4 XRD diffraction patterns of MA, WMSN and 65 wt% MA/WMSN composite.

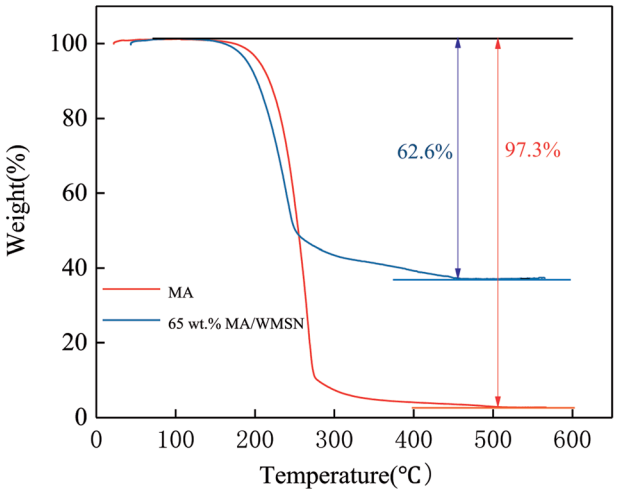

Fig. 6 TGA curves of MA, 65 wt% MA/WMSN.

channels.[12,15,21] Fig. 3(b) shows that the most of the pore-size distribution of WMSN was between 3 nm and 6 nm. The BJH cumulative pore volume of adsorption was 0.895 $cm^3\ g^{-1}$. The BET (Brunauer–Emmett–Teller) specific surface area was evaluated to be 574.144 $m^2\ g^{-1}$. The BJH adsorption pore size was 3.086 nm. The above data indicated that WMSN had large specific surface area and pore volume, which could increase the loading amount of MA in the shape-stabilized phase change material and enhance its phase change enthalpy.

Crystallization properties of MA and MA/WMSN

Fig. 4 indicates the XRD diffraction patterns of MA, WMSN and MA/WMSN composite, and the different peaks were in the same unit. The pattern of MA showed two intensive sharp diffraction peaks at approximately 21.6° and 24.1° because of its crystalline structure. The XRD patterns of the WMSN showed that between 20° and 30° there was a wide peak. This phenomenon suggested that the WMSN had an amorphous structure.[22] The XRD pattern of the MA/WMSN composite showed that the similar diffraction

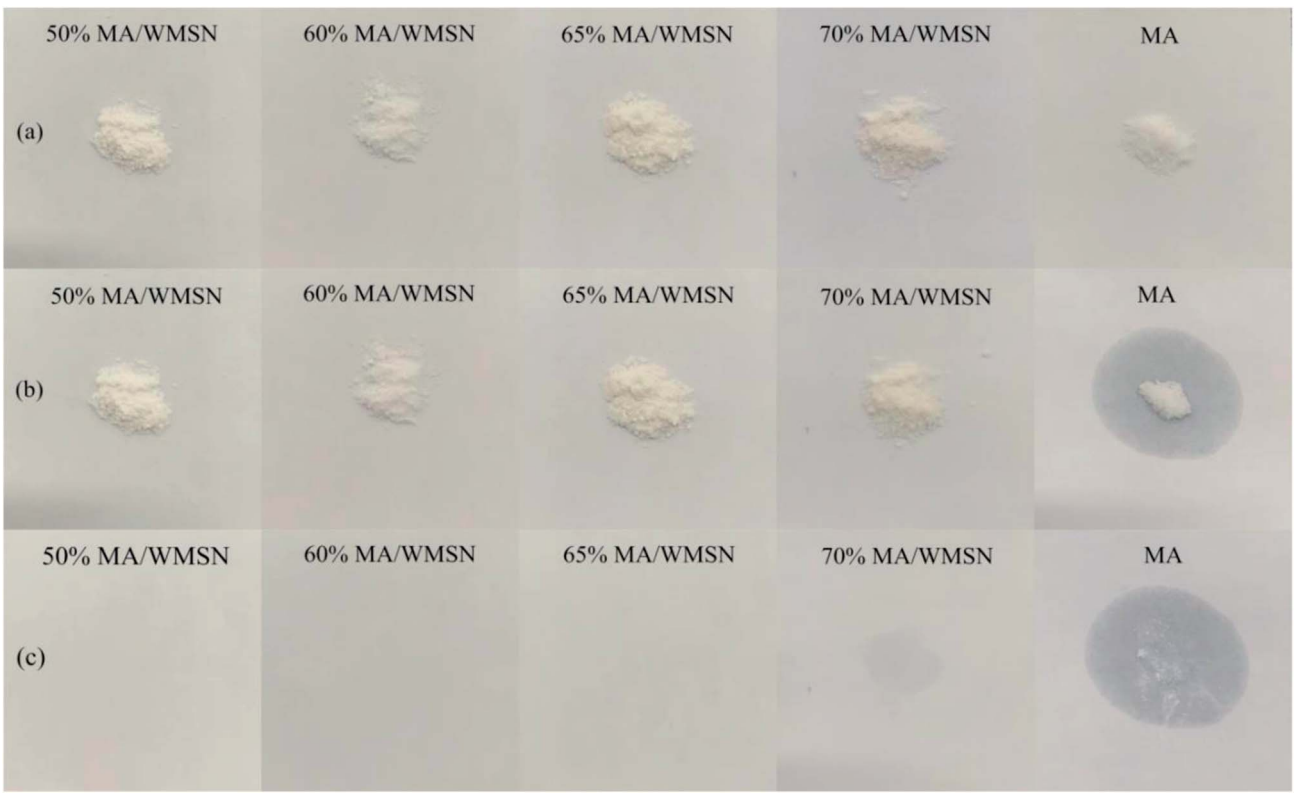

Fig. 5 Photographs of (a) MA/WMSN and pristine MA at room temperature; (b) MA/WMSN and pristine MA at 64 °C; (c) leakage of MA/WMSN and pristine MA at 64 °C.

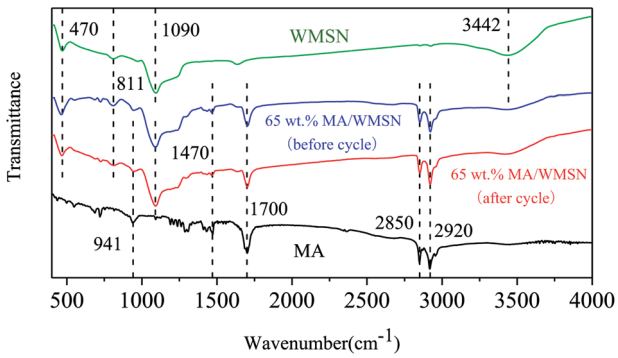

Fig. 7 FT-IR spectra of MA, WMSN, and 65 wt% MA/WMSN before and after 50 cycles.

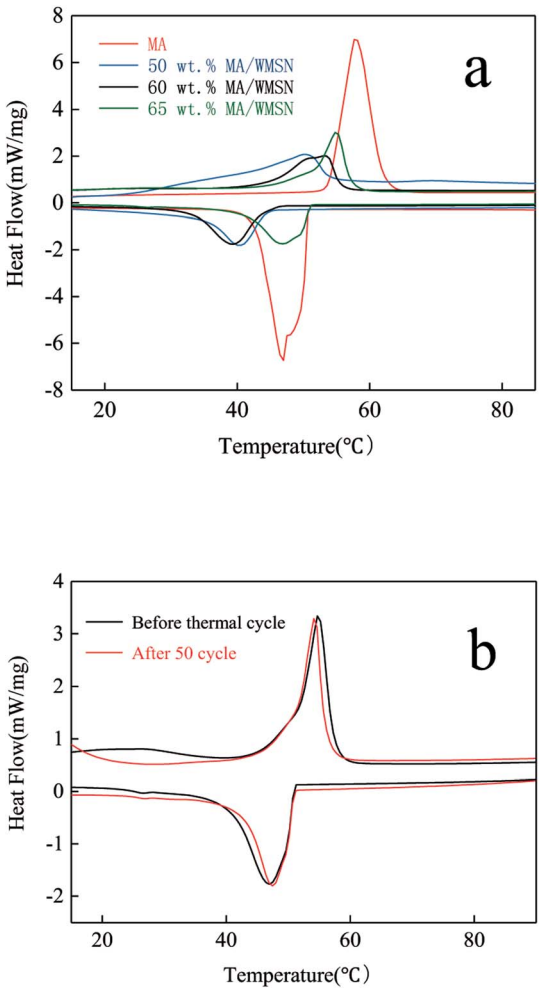

Fig. 8 DSC analysis of (a) MA and MA/WMSN composite with different contents and (b) 65 wt% MA/WMSN before and after 50 thermal cycles.

peaks of MA and the wide peak of WMSN were also present in MA/WMSN. This finding suggests that MA/WMSN contained the crystal structure of MA and the amorphous structure of WMSN, and moreover, it was demonstrated that the crystal structure of MA was complete and that there was no chemical reaction between MA and WMSN.[23] Obviously, the peaks of MA/WMSN were lower than the peaks of MA at 21.6° and 24.1°, and this phenomenon might be attributed to the slight influence for the MA by the capillary force between the MA and the WMSN.[24] The appearance of the sharp diffraction peaks from MA meant that the WMSN had no restrictive state over MA molecular chains.[24]

Table 1 Thermal characteristics of MA and prepared MA/WMSN

	Endothermic peak		Exothermic peak	
Samples	H_{en} (J g^{-1})	T_{en} (°C)	H_{ex} (J g^{-1})	T_{ex} (°C)
MA	184.3	57.7	197.2	47.0
50 wt% MA/WMSN	69.2	50.4	64.9	40.5
60 wt% MA/WMSN	87.1	53.4	77.6	39.4
65 wt% MA/WMSN	92.0	54.7	86.0	46.9

Leakage tests of MA/WMSN

The leakage tests for determining and comparing the stabilities of pure MA, 50 wt%, 60 wt%, 65 wt%, and 70 wt% MA/WMSN were performed by placing them into a baking oven for 10–15 min at 69 °C to check whether they would leak, and the results are shown in Fig. 5. Pure MA was melted at a certain temperature higher than the melting point of MA. However, no leakage was observed for the 65 wt% MA/WMSN in the same environment, which benefited from the numerous merits of WMSN, including the special and highly uniform morphology with wrinkled channels, high specific surface area, large pore volume and high porosity. A slight leakage was observed for the 70 wt% MA/WMSN. Therefore, the 65 wt% MA/WMSN was studied as the main shape-stabilized PCM in the following experiments.

Thermal stabilities of MA and MA/WMSN

Thermal stabilities of MA and MA/WMSN were analyzed and the amount of adsorptive MA in the WMSN was estimated by TGA. The TGA curves of pure MA and 65 wt% MA/WMSN composite are revealed in Fig. 6. In Fig. 6, the TGA curves showed that the process of the losing weight for MA and MA/WMSN occurred in only one step. The TGA curve of MA showed that initial weight loss started at 180 °C, and when the temperature rose to approximately 475 °C, the MA decomposed with 2.7 wt% unknown remains, which might be related to the weighing error and impurities. The TGA curve of 65 wt% MA/WMSN shows that the weight loss of MA/WMSN was 62.6 wt%, and it was nearly in accordance with the theoretical calculation, which indicated that the prepared MA/WMSN composite was a uniform product. It could be seen from Fig. 6 that there was distinct weight loss at the temperature range of approximately 180 °C to 250 °C, which was because of the disintegration of molecular chains. Moreover, the decomposition temperature of 65 wt% MA/WMSN was lower than that of the pure MA, and this result might be caused by the improvement of the thermal conductivity of 65 wt% MA/WMSN, which could enhance its heating rate and decomposing rate, and then its decomposition temperature was decreased.

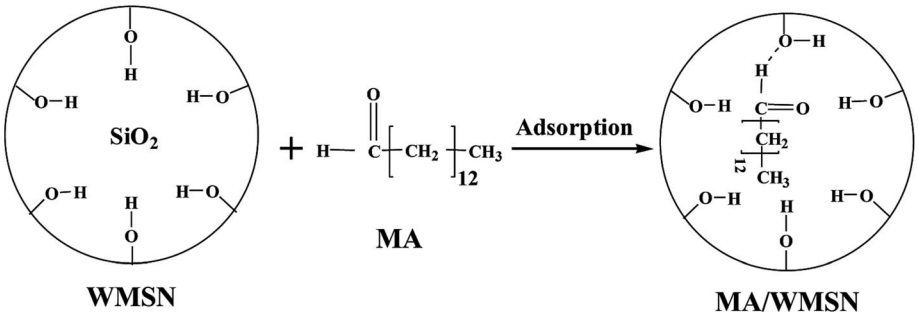

Fig. 9 Schematic illustration of the interaction mechanism of MA molecule and WMSN in the MA/WMSN composite.

This was in accordance with the study results reported by other researchers.[25,26] However, there was no significant weight loss and decomposing reaction from 20 °C to approximately 180 °C, which indicated that the MA/WMSN composite had excellent thermal stability.

FT-IR analysis of MA and MA/WMSN

Fig. 7 shows the FT-IR spectra of MA, WMSN, and 65 wt% MA/WMSN before and after 50 cycles. In the spectrum of MA, the peaks located at 2850 cm^{-1} and 2920 cm^{-1} were caused by antisymmetric and symmetric stretching vibrations of C–H.[27,28] The peak located at 941 cm^{-1} corresponded to the –OH vibration mode,[29] and the C–H rocking vibration was observed at 1470 cm^{-1}.[27] In addition, the peak at 1700 cm^{-1} belonged to the C=O stretching vibration.[30,31] In the WMSN spectrum, the peak at 1090 cm^{-1} was due to the asymmetric stretching vibration mode of Si–O–Si functional groups,[32] and the peaks at 470 cm^{-1} and 811 cm^{-1} were ascribed to the deformation patterns and symmetric stretching of Si–O–Si.[21] The peak at 3442 cm^{-1} was affected by the rocking vibration of the water molecule or the OH groups.[32,33] In the spectrum of MA/WMSN, we could locate all of the peaks in the curves of both MA and WMSN, and there was no obvious new peak, which indicated that the interaction between MA and WMSN was only physical, and the adsorption between MA and WMSN was successful. Moreover, compared with the spectra of 65 wt% MA/WMSN before and after thermal cycles, it could be found that there was no obvious change in the shape and position of the major peaks for 65 wt% MA/WMSN after 50 cycles, which suggested that the 65 wt% MA/WMSN had a good chemical stability with a long life cycle.

Thermal properties of MA and MA/WMSN

Thermal properties, including the phase change temperature and enthalpies of the core material and the MA/WMSN composites, were determined by DSC. Fig. 8 a and Table 1 show the DSC analysis results of MA and MA/WMSN composite with different contents. Fig. 8 shows that the melting temperature and crystalline temperature ranged from 38 °C to 58 °C, which meant that those MA/WMSN with different contents of MA had similar reversible and balanced phase change behaviors for MA. According to the results in Table 1, pure MA had an endothermic and exothermic peak at 57.7 °C and 47.0 °C, respectively. The melting and crystallizing enthalpies were 184.3 J g^{-1} and 197.2 J g^{-1}, respectively. In Fig. 8a, the peak area of MA/WMSN was smaller than that of pure MA. Furthermore, with increased MA content, the exothermic peak area of MA/WMSN became larger, and the enthalpy of MA/WMSN composite also increased. Meanwhile, the position of the peaks moved towards a higher temperature, which was related to the content of MA. The DSC curve of the 50 wt% MA/WMSN became flat, meaning that the enthalpy was very small. The melting and crystallizing enthalpies of the 65 wt% MA/WMSN were 92 J g^{-1} and 86 J g^{-1}, respectively. The practical enthalpies of MA/WMSN were lower than the theoretical enthalpies, which was attributed to the capillary force between MA and WMSN.[24] In addition, MA/WMSN is hydrophilic with hydroxyl ends,[34] and the hydrogen bonds formed between the MA molecules and Si–OH on the surface of WMSN would restrict the crystallization behavior of MA.[35] Therefore, the movement of MA chains was restricted partly by the capillary force and hydrogen bonds between MA and WMSN.[11,24] The interaction mechanism of MA molecule and WMSN in the MA/WMSN composite is shown in Fig. 9. Additionally, compared

Table 2 Parameters of thermal diffusivities α, specific heat capacities C_p and thermal conductivities K of MA and MA/WMSN

Samples	α ($cm^2\ s^{-1}$)	C_p (J g^{-1} °C^{-1})	K (W mK^{-1})
MA	0.15×10^{-2}	1.86	0.27
65 wt% MA/WMSN	0.18×10^{-2}	1.71	0.37

Table 3 Comparison of the thermal conductivity of 65 wt% MA/WMSN with other composite materials

Samples	K (W mK^{-1})	Ref.
65 wt% MA/WMSN	0.37	This study
FSPCM-E5[a]	0.14	Chen *et al.*[24]
HPCM2(70% MA)[b]	0.2038	Tang *et al.*[27]
CA[c]-MA/VMTCA[d]	0.22	Karaipekli *et al.*[36]
60% PEG[e]/ZSM-5[f]	0.54	Li *et al.*[37]
CA-MA/PMMA[g]	0.269	Meng *et al.*[38]

[a] 50% MA/Eudragit L100. [b] Capric acid. [c] Vermiculite. [d] $Na_nAl_nSi_{96}$–$nO_{192}\cdot 16H_2O(0 < n < 27)$. [e] Poly-methyl methacrylate. [f] $Na_nAl_nSi_{96}$–$nO_{192}\cdot 16H_2O(0 < n < 27)$. [g] Poly-methyl methacrylate.

Table 4 Comparison of the phase change properties of 65 wt% MA/WMSN with other composite materials

	Endothermic peak		Exothermic peak		
Samples	H_{en} (J g^{-1})	T_{en} (°C)	H_{ex} (J g^{-1})	T_{ex} (°C)	Ref.
65 wt% MA/WMSN	92.0	54.7	86.0	46.9	This study
FSPCM-B5[a]	53.2	52.5	56.2	48.5	Chen *et al.*[24]
FSPCM-E6[b]	85.9	51.4	88.3	52.4	Chen *et al.*[24]
PEG/ZSM-5[c]	76.4	56.3	64.3	44.9	Li *et al.*[37]
MW-FSPCM[d]	99.6	51.2	98.7	52.7	Jiang *et al.*[39]
75 wt% PEG[e]/SF[f]	81.3	56.9	76.5	24.1	Wang *et al.*[40]

[a] 50 wt% MA/bentonite. [b] 60 wt% MA/Eudragit L100. [c] 50 wt% PEG/$Na_nAl_nSi_{96}$–$nO_{192}\cdot 16H_2O$($0 < n < 27$). [d] 60 wt% MA/wood-flour. [e] Poly ethylene glycol. [f] 75 wt% PEG/silica fume.

with the MA curve, the peak of MA/WMSN was wider, which was related to the impediment of heat transformation caused by the interface between MA and WMSN in MA/WMSN.[23]

The thermal cycle experiments were carried out for determining the thermal reliability of MA/WMSN, and Fig. 8b shows the DSC curves of 65 wt% MA/WMSN before and after 50 cycles. The thermal cycle test results indicated that the phase change temperature and enthalpies of 65 wt% MA/WMSN had a slight change before and after 50 thermal cycles, which suggested that the 65 wt% MA/WMSN had a good thermal reliability.

Thermal conductivities of MA, WMSN and MA/WMSN

Thermal conductivity is an important parameter for the thermal energy storage materials. The thermal conductivities, thermal diffusivities and specific heat capacities of MA and MA/WMSN are shown in Table 2, and the thermal conductivities of MA and 65 wt% MA/WMSN were 0.27 and 0.37 W (mK)$^{-1}$, respectively. Compared with pure MA, the thermal conductivity of MA/WMSN was enhanced by 37.04%, which demonstrated that the addition of WMSN improved the heat transfer rate of MA/WMSN, and therefore, the MA/WMSN had more efficient energy utilization.

The thermal conductivity and phase change properties of other shape-stabilized PCMs are shown in Table 3 and 4 respectively in order to compare them with that of the 65 wt% MA/WMSN synthesized in this study. Although the thermal conductivity and phase change properties of the MA/WMSN were not the best, its performance was competitive. Additionally, MA/WMSN possessed of favourable thermal conductivity and excellent thermal stability, and therefore, it had great potential in the application of thermal energy storage.

Conclusions

In this study, wrinkled mesoporous silica nanoparticle (WMSN) was prepared and used as the supporter of myristic acid (MA) for preparing a new shape-stabilized PCM (MA/WMSN), and the MA/WMSN was prepared by a vacuum impregnation method, which was simple and easy to operate. According to the results of characterization tests, the WMSN had a special radial wrinkled morphology, and the wrinkled channels were beneficial to prevent the leakage of PCM. The BJH cumulative pore volume of adsorption was 0.895 cm^3 g^{-1}, and the pore size was 3.086 nm. Furthermore, the interaction between MA and WMSN was only physical. The highest load of MA in MA/WMSN was 65%, and its melting and crystallizing enthalpies were 92.0 J g^{-1} and 86.0 J g^{-1}, respectively. Furthermore, the thermal conductivity of MA/WMSN was enhanced effectively, and it was about 1.37 times higher than that of the pure MA. The characterizations results indicated that the MA/WMSN possessed favourable thermal conductivity, high latent heats and excellent thermal stability, and thus we envision that it had great potential to be used as a suitable thermal energy storage material for practical applications. Additionally, the WMSN with large specific surface area, high porosity and radial-like wrinkled channels synthesized in this study could also be used as the matrix of other organic phase change materials such as paraffin wax, hexadecane, stearic acid and so on to prepare shape-stabilized PCMs.

Conflicts of interest

The authors declare no Conflict of Interest.

Acknowledgements

The authors are grateful for the financial supports of the Zhejiang Provincial Natural Science Foundation of China (No. LY18E060007) and the National Natural Science Foundation of China (No. 51606168).

Notes and references

1 X. Zong, Y. B. Cai, G. Y. Sun, Y. Zhao, F. L. Huang and L. Song, *Sol. Energy Mater. Sol. Cells*, 2015, **132**, 183–190.
2 M. D. Kilde, P. G. Arroyo, A. S. Gertsen, K. V. Mikkelsen and M. B. Nielsen, *RSC Adv.*, 2018, **8**, 6356–6364.
3 I. Sarbu and C. Sebarchievici, *Sustainability*, 2018, **10**, 191.
4 Y. Chen, X. J. Zhang, B. F. Wang, M. J. Lv, Y. Y. Zhu and J. K. Gao, *RSC Adv.*, 2017, **7**, 15625–15631.
5 X. Min, M. H. Fang, Z. H. Huang, Y. G. Liu, Y. T. Huang, R. L. Wen, T. T. Qian and X. W. Wu, *Sci. Rep.*, 2015, **5**, 12964.
6 T. T. Qian, J. H. Li, H. W. Ma and J. Yang, *Polym. Compos.*, 2016, **37**, 854–860.

7 X. G. Zhang, Z. H. Huang, B. Ma, R. L. Wen, X. Min and Y. T. Huang, *Thermochim. Acta*, 2016, **638**, 35–43.
8 J. M. Maldonado, M. Fullana-Puig, M. Martín, A. Sole, A. G. Fernandez, A. Gracia and L. F. Cabeza, *Energies*, 2018, **11**, 861.
9 A. B. Rezaie and M. Montazer, *Appl. Energy*, 2018, **228**, 1911–1920.
10 H. Z. Ke, *Appl. Therm. Eng.*, 2017, **113**, 1319–1331.
11 T. T. Qian, J. H. Li, W. W. Feng and H. E. Nian, *Energy Convers. Manage.*, 2017, **143**, 96–108.
12 J. J. Wang, M. Yang, Y. F. Lu, Z. K. Jin, L. Tan, H. Y. Gao, S. Fang, W. J. Dong and G. Wang, *Nano Energy*, 2016, **19**, 78–87.
13 T. T. Qian, J. H. Li, X. Min, Y. Deng, W. M. Guan and L. Ning, *Energy*, 2016, **112**, 1074–1083.
14 T. Kadoono and M. Ogura, *Phys. Chem. Chem. Phys.*, 2014, **16**, 5495–5498.
15 A. M. Goitandia and G. Beobide, *Sol. Energy Mater. Sol. Cells*, 2015, **134**, 318–328.
16 D. S. Moon and J. K. Lee, *Langmuir*, 2012, **28**, 12341–12347.
17 J. Gao, W. X. Kong, L. Y. Zhou, Y. He, L. Ma, Y. Wang, L. Y. Yin and Y. J. Jiang, *Chem. Eng. J.*, 2017, **309**, 70–79.
18 N. I. Vazquez, Z. Gomzalez, B. Ferrari and Y. Castro, *Bol. Soc. Esp. Ceram. Vidrio*, 2017, **56**, 139–145.
19 D. S. Moon and J. K. Lee, *Langmuir*, 2014, **30**, 15574–15580.
20 H. Yang, S. J. Liao, C. Huang, L. du, P. chen, P. Y. Huang, Z. Y. Fu and Y. W. Li, *Appl. Surf. Sci.*, 2014, **314**, 7–14.
21 J. Gao, W. X. Kong, L. Y. Zhou, Y. He, L. Ma, Y. Wang, L. Y. Yin and Y. J. Jiang, *Chem. Eng. J.*, 2017, **309**, 70–79.
22 G. X. Cao, J. Gao, L. Y. Zhou, Z. H. Huang, Y. He, M. Zhu and Y. J. Jiang, *Biochem. Eng. J.*, 2017, **128**, 116–125.
23 J. L. Zeng, F. R. Zhu, S. B. Yu, Z. L. Xiao, W. P. Yan, S. H. Zheng, L. Zhang, L. X. Sun and Z. Cao, *Sol. Energy Mater. Sol. Cells*, 2013, **114**, 136–140.
24 C. Z. Chen, X. D. Liu, W. M. Liu and W. F. Ma, *Sol. Energy Mater. Sol. Cells*, 2014, **127**, 14–20.
25 R. R. Cao, X. Li, S. Chen, R. R. Yuan and X. X. Zhang, *Energy*, 2017, 138.
26 B. Wu, Y. Y. Jiang, Y. J. Wang, C. L. Zhou, X. Zhang and J. X. Lei, *Int. J. Heat Mass Transfer*, 2018, **126**, 1134–1142.
27 Y. J. Tang, D. Su, X. Huang, G. Alva, L. K. Liu and G. Y. Fang, *Appl. Energy*, 2016, **180**, 116–129.
28 A. Karaipekli and A. Sari, *Renewable Energy*, 2008, **33**, 2599–2605.
29 S. Ince, Y. Seki, M. A. Ezan, A. Turgut and A. Erek, *Renewable Energy*, 2015, **75**, 243–248.
30 G. Y. Fang, H. Li, Z. Chen and X. Liu, *Energy*, 2010, **35**, 4622–4626.
31 M. Ferreira, K. Wohnrath, A. Riul, J. A. Giacometti and O. N. Oliveira, *J. Phys. Chem. B*, 2002, **106**, 7272–7277.
32 R. A. Mitran, D. Berger and C. Matei, *Thermochim. Acta*, 2018, **660**, 70–76.
33 L. Zhang, P. Zhang, F. Wang, M. Kang, R. Q. Li, Y. R. Mou and Y. H. Huang, *Appl. Therm. Eng.*, 2016, **101**, 217–223.
34 X. Y. Huang, P. Z. Liu, W. Xia, R. Q. Zhou and R. D. S. Han, *J. Mater. Chem. A*, 2015, **3**, 1935–1940.
35 W. Aftab, X. Y. Huang and R. Q. Zou, *Energy Environ. Sci.*, 2018, **11**, 1392–1424.
36 A. Karaipekli and A. Sari, *Sol. Energy*, 2009, **83**, 323–332.
37 C. E. Li, H. Yu, Y. Song and M. Zhao, *Renewable Energy*, 2017, 121.
38 D. Meng and L. J. Wang, *J. Wuhan Univ. Technol., Mater. Sci. Ed.*, 2013, **28**, 586–591.
39 L. Jiang, Z. M. Liu, Y. Yuan, Y. J. Wang, J. X. Lei and C. L. Zhou, *Energ. Buildings*, 2018, **171**, 88–99.
40 C. L. Wang, K. L. Yeh, C. W. Chen, Y. Lee, H. L. Lee and T. Lee, *Appl. Energy*, 2017, **191**, 239–250.